Monolayers

DOI: 10.1002/anie.201001064

Nanotexture Switching of Single-Layer Hexagonal Boron Nitride on Rhodium by Intercalation of Hydrogen Atoms**

*Thomas Brugger, Haifeng Ma, Marcella Iannuzzi, Simon Berner, Adolf Winkler, Jürg Hutter, Jürg Osterwalder, and Thomas Greber**

The appearance, response, and functionality of a surface are determined by its texture. At the nanoscale, the texture rules the arrangement of molecules and their equilibrium with the gas phase. New applications are expected if the texture can be switched between different states. Herein, we show that atomic hydrogen acts as an agent for the control of the corrugation of a single layer of hexagonal boron nitride (*h*-BN) on a rhodium metal support. The hydrogen atoms intercalate between the sp^2 hybrid layer and the metal by substitution of the bonds between *h*-BN and the substrate.

Intercalation, that is, the reversible embedding of atomic or molecular species in a layered material, is a key concept in materials functionalization. Graphite is the prototype intercalation material,[1] in which the relatively weak bonding between sp^2-hybridized carbon sheets allows the packing of atomic or molecular species between adjacent layers. Single sheets of carbon (graphene) and *h*-BN form highly ordered nanostructures on transition metals.[2–5] The lateral periodicity of these superstructures is determined by the lattice mismatch between the sp^2 layers and the substrate. For 4d and 5d transition metals, the superlattice constant is about 10 times that of the free-standing sp^2 layer. The deformation of the surfaces in the vertical direction, that is, the corrugation, can reach values of 0.15 nm and is controlled by the bonding of B, C, and N to the transition metals, where the lattice mismatch and the site dependent bonding impose a dislocation network with mainly out-of-plane strain in the sp^2 layer. The corrugation is the essential property that determines the texture and functionality of these superstructures with a variety of new phenomena such as the formation of dipole rings, which impose in-plane lateral electric fields[6,7] that constitute traps for single molecules or clusters at room temperature.[8,9] The *h*-BN/Rh(111) nanomesh[4] model system has a superlattice constant of 3.2 nm and displays a meshlike morphology, where the "holes" or "pores" of the mesh with a diameter of 2 nm are regions with close contact to the substrate, and where the "wires" are loosely bound to the substrate.[8] We have shown that the height difference between the holes and the wires, that is, the corrugation, of approximately 0.1 nm may be reversibly switched off and on from corrugated to flat by hydrogen intercalation and hydrogen removal. This finding is expected to have implications for applications such as hydrogen storage, switching of surface properties like a template function, or the peeling of sp^2-hybridized layers from solid substrates such as hexagonal boron nitride or graphene.

The *h*-BN/Rh(111) nanomesh superstructure can be directly observed by using STM. The nanomesh has a peculiar electronic structure that is reflected in the core level binding energies of the elements, which are sensitive to the position of the atoms.[10] A splitting of the N 1s core level into two components as observed by X-ray photoelectron spectroscopy (XPS) is ascribed to the *h*-BN layer corrugation,[10] and a separate set of sp^2-derived bands is observed by ultraviolet photoelectron spectroscopy (UPS).[4]

The topographic STM data in Figure 1 show a *h*-BN nanomesh after exposure to atomic hydrogen, which leads to a partial removal of the corrugation. A new phase of single-layer *h*-BN without long-range periodic corrugation (2) coexists with the unaltered nanomesh (1). Phase 2 is basically flat whereas the pristine nanomesh (1) exhibits the corrugated hexagonal surface with a periodicity of 3.2 nm.[11] The expanded images in Figure 1 show sections taken from regions with and without corrugation. In the first expansion (Figure 1b), eight nanomesh unit cells are seen, where the two topographic elements, the "holes" (*H*) and the "wires" (*W*) become visible. The expansion of the flat region shows no corrugation at the length scale of 3 nm (Figure 1c). The height profile in Figure 1d shows the transition from the intact, corrugated nanomesh region into the flat region. The surface in the flat region levels on the height of the "wires", that is, the loosely bound regions in the nanomesh. Compared with a recent report on the saturation of graphene on SiC by atomic hydrogen and an adsorption-induced change of the surface morphology,[12] the present effect involves hydrogen intercalation, that is, bonding to the transition metal substrate, which removes the intrinsic nanoscale pattern of *h*-BN/Rh(111). The effect is caused by atomic hydrogen or deuterium, and, at the investigated low-pressure conditions, not by the molecular forms H_2 or D_2.

[*] Dr. T. Brugger, Dr. H. Ma, Dr. S. Berner, Prof. Dr. J. Osterwalder, Prof. Dr. T. Greber
Physik-Institut, Universität Zürich
Winterthurerstrasse 190, 8057 Zürich (Switzerland)
E-mail: greber@physik.uzh.ch
Homepage: http://www.physik.uzh.ch/groups/grouposterwalder/index.php
Dr. M. Iannuzzi, Prof. Dr. J. Hutter
Physikalisch Chemisches Institut, Universität Zürich
Winterthurerstrasse 190, 8057 Zürich (Switzerland)
Prof. Dr. A. Winkler
Institute of Solid-State Physics, Graz University of Technology
Petersgasse 16, 8010 Graz (Austria)

[**] We thank Dr. A. P. Seitsonen for stimulating discussions and help with the representation of the theoretical structure optimization results. M.I. and H.M. acknowledge funding by the Sinergia program of the Swiss National Science foundation.

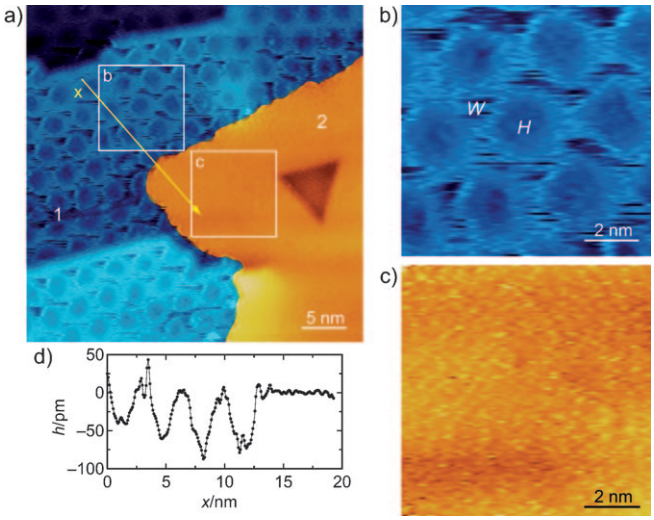

Figure 1. Topographic STM data of *h*-BN/Rh(111) after exposure to atomic hydrogen. The color coding emphasizes two distinct nanotextures. a) Large-scale image showing the coexistence of corrugated and hydrogen intercalated flat *h*-BN/Rh(111) (regions 1 and 2 respectively). The dark triangle in region 2 is a dislocation within the Rh(111) substrate was used as a landmark for orientation. b) Expansion of the pristine *h*-BN/Rh(111) nanomesh area showing the wire (W) and the hole (H) regions. c) Expansion of the flat *h*-BN/Rh(111) area. d) Line profile along the yellow line *x* in (a) showing the transition from corrugated (1) to flat (2) *h*-BN/Rh(111).

In order to determine the amount of hydrogen or deuterium that is incorporated into *h*-BN/Rh(111) in the flat state, we performed thermal desorption spectroscopy (TDS) measurements during annealing, which leads to the restoration of the corrugation. We found no isotope effect between H and D atoms, although it is advantageous to use D because of a lower background signal. Figure 2 shows the TDS curve of molecular deuterium (heating rate 0.2 $K s^{-1}$) from a sample that had been exposed to D atoms in order to switch off the corrugation. The sample was subsequently flushed with H_2 in order to supplant D atoms on the sample holder by an isotope-exchange reaction. At these low temperatures, no desorption of atomic D atoms is expected, though

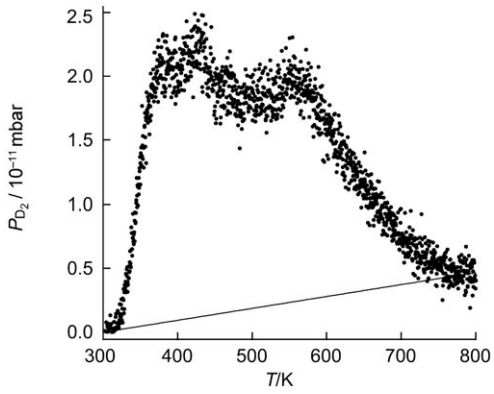

Figure 2. Deuterium thermal desorption spectrum from *h*-BN/Rh(111) exposed to atomic D (heating rate 0.2 $K s^{-1}$). The area above the solid line was used for quantification.

desorbing D_2 may exchange with the hydrogen on the walls of the experimental chamber to form HD. The TDS signal of HD (atomic mass 3 Da) was therefore simultaneously recorded. From the area under both curves (3 Da and 4 Da) and the pumping speed, an amount of desorbed D atoms can be inferred. With this value and the sample area, we find the D-atom density n_D to be approximately $(4 \pm 0.5 \times 10^{14})$ cm^{-2} in the flat state. This value of n_D corresponds to about 0.25 ML (1 ML = one atom per top-layer Rh atom). It has to be regarded as a lower limit for the incorporated D atoms, because the increasing D_2 and HD background, as well as possible diffusion of D atoms into Rh, is not counted. However, the value of n_D is remarkably close to the number of protons that was found to bind to *h*-BN/Rh(111) in an electrolyte.[13] The low desorption temperature indicates a relatively low binding energy of D atoms in *h*-BN/Rh(111). The reproducible double-peak structure in the TD spectra suggests kinetics beyond a model with a single activation energy.

The surface texture switching was further monitored by photoemission, that is, the N 1s and B 1s core-level spectra and the splitting of the sp^2-derived valence bands (Figure 3). The evolution of the N 1s core-level peak during a switch-off/switch-on cycle substantiates the switching process (Figure 3a). The N 1s peak of the nanomesh can be fitted by two equally wide Gaussians with a splitting of 680 meV between a low and a high binding energy component which correspond to the nitrogen in the wire (N_W) and in the hole region (N_H), respectively.[10] The fit results in a N_W/N_H ratio of about 3:1. After flattening of the nanomesh by hydrogen, the peak considerably narrowed at the binding energy of the wire regions. Upon annealing, the N 1 s peak broadens back to the original ratio of $N_W/N_H \approx 3{:}1$. The same effect is observed for the B 1 s core level (not shown), though the splitting is smaller. These X-ray photoelectron spectroscopy (XPS) results are an indication that the hydrogen does not bind to the *h*-BN, and it is thus conjectured that the H atoms intercalate, that is, bind to the Rh substrate. The insets in Figure 3a) show low-energy electron diffraction (LEED) data of the nanomesh in the two states. Within the accuracy of the experiment, the supercell size does not depend on the corrugation. The superstructure diffraction spots in the corrugated case correspond to (13×13) *h*-BN on (12×12) Rh units. The sharpness and positions of the diffraction spots in the flat phase prove the structural integrity of the *h*-BN layer and exclude a twist with respect to the Rh(111) substrate. The $He\,I_\alpha$ photoemission spectra (Figure 3b) also indicate a flattening of the *h*-BN layer: the bands related to the holes of the nanomesh (σβ and πβ) vanish after exposure to H atoms. Furthermore, annealing of the H-exposed sample (H/*h*-BN/Rh(111)) to about 600 K results in recovery of the original band splitting, which arises from the switch back to the pristine nanomesh.

The calculated density of states (DOSs) of p_x states on the nitrogen atoms that constitute the *h*-BN σ bands are displayed in Figure 3c,d. The results for the clean nanomesh (Figure 3c) are consistent with those reported in references [8,14]. The N p_x DOS in the hole and the wire sites have pronounced peaks at about 7 eV and 6 eV below the Fermi

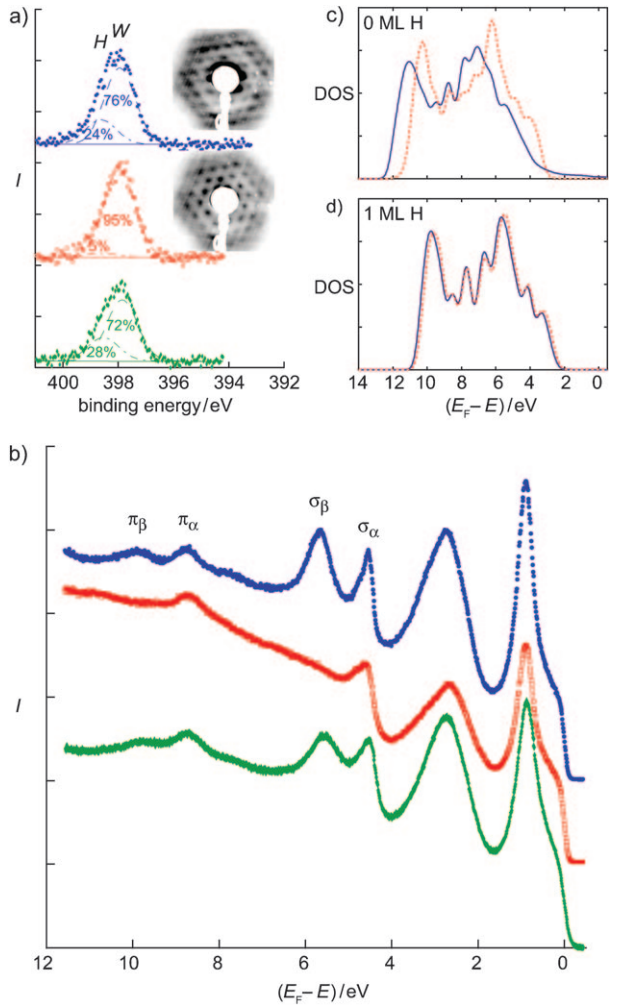

Figure 3. a,b) The *h*-BN/Rh(111) nanomesh before (filled blue circles; pristine *h*-BN/Rh(111)) and after hydrogenation (open red squares; H/*h*-BN/Rh(111)), and after H desorption (filled green diamonds; healed *h*-BN/Rh(111)). a) N 1s core level XPS (monochromatized Al Kα radiation), which features a distinct narrowing upon hydrogenation. The insets show the low energy electron diffraction (LEED) patterns of the corrugated superstructure of *h*-BN/Rh(111) (upper panel) and the superstructure of H/*h*-BN/Rh(111) (lower panel) for a primary electron energy of $E = 12.9$ eV. b) He I_α normal emission ultraviolet photoemission spectrum (UPS) shows a vanishing of the σβ and πβ peaks that are attributed to the holes (*H*) of *h*-BN/Rh(111) after exposure to H atoms, while the σα and πα peaks corresponding to the wires (*W*) of the *h*-BN/Rh(111) remain. c, d) Calculated projected DOS of p_x orbitals originating from N atoms in hole (solid blue line) and wire (dashed red line) regions of pristine (0 ML) *h*-BN/Rh(111) and d) *h*-BN/Rh(111) intercalated with 1 ML H atoms.

energy E_F, which are consistent with the experimentally observed σ-band splitting of about 1 eV. The calculated densities in Figure 3d comprise one monolayer of intercalated hydrogen and feature the experimentally observed disappearance of the hole-derived σβ band in *h*-BN/Rh(111) under the exposure to H (or D) atoms. The theoretical σ-band peak splitting depends in a nonlinear fashion on the hydrogen coverage, which is 0.9, 0.4, 0.26 and 0.22 eV for 0, 0.25, 0.5 and 1 ML of intercalated hydrogen, respectively. Given that the theoretical σ-band peak splitting between 0.5 and 1 ML does not greatly decrease, this result implies that the UPS data without σ-band splitting can also be described with 0.5 ML intercalated H atoms, which agrees better with the TDS data. Also, a coverage of 0.5 ML H atoms reduces the discrepancy with respect to the σα binding energy between the experimental and theoretical results. When referenced to the Fermi level, theoretical results predict an upshift of the σ bands of about 0.7 eV per ML H atoms, while the experimental evidence indicates no sizeable σα-band energy shift.

The structure of the full *h*-BN/Rh(111) system was optimized by DFT calculations with 567 Rh atoms and 169 BN pairs in the unit cell. The results for the hydrogen-free *h*-BN/Rh(111) are consistent with previously reported results.[14] The overall binding of the *h*-BN layer is −0.29 eV per BN pair. The optimized structure (Figure 4a) shows a

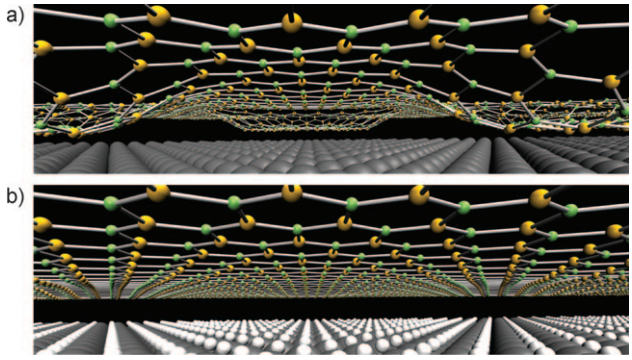

Figure 4. 3D representation of the results from the structure optimizations with DFT. a) Pristine *h*-BN/Rh(111). b) *h*-BN/Rh(111) with one H atom per Rh unit intercalated between the *h*-BN and the topmost Rh(111) layer. The corrugation amplitude of the *h*-BN layer is enhanced by a factor of two in the pictures. Rh gray, B orange, N green, H white. Atom sizes are not to scale.

corrugated *h*-BN layer where about 30% of the BN units are in close contact and about 60% are in loose contact with the Rh(111) substrate (about 2.2 Å and 3.2 Å above the topmost Rh(111) layer). The remaining 10% of the BN units are assigned to the "rims" between holes and wires. Intercalation of H atoms below *h*-BN on Rh(111) has been investigated in several steps, starting with a single H atom on top of a free-standing *h*-BN layer, where no binding was found for distances greater than 2 Å. On bare Rh(111), H bonding is calculated up to one monolayer, where the binding energy per H atom decreases with coverage (−2.87 eV for 0.25 ML, −2.82 eV for 0.5 ML, −2.74 for 1 ML). H atoms slightly favor face-centered cubic (fcc) hollow sites (−2.74 eV per H atom for 1 ML fcc versus −2.72 eV for 1 ML hexagonal close-packed (hcp)), which is consistent with the data in reference [15]. In the case of *h*-BN/Rh(111), the H atoms are distributed with different densities (0.25, 0.5, and 1 ML) on either fcc or hcp sites between the *h*-BN and the top Rh layer. The full system of 13×13 BN units and a four-layer 12×12 Rh(111) slab in the presence of intercalated H has been optimized. All structure optimizations led to H-bonding configurations, where the mean distance between *h*-BN layer and Rh increases with H density, and where the

corrugation reduces gradually. Although the H-binding energies are only weakly dependent on coverage and adsorption sites (fcc or hcp), H-binding energies of −2.57, −2.59, and −2.62 eV for 0.25, 0.5 and, 1 ML H atoms are found for the fcc sites. Again, the hcp sites are marginally less favored (−2.60 eV at 1 ML coverage). The binding energy of H atoms intercalated between *h*-BN and Rh(111) is weaker with respect to bare Rh(111), where the difference is close to the average *h*-BN-Rh(111) bond energy. This result indicates the subtle balance between H-Rh and BN-Rh bonding, which is only slightly favorable for H/Rh, but enables the switching of the texture of *h*-BN-Rh(111). The resulting structure for 12×12 intercalated H atoms per supercell unit (1 ML) is shown in Figure 4b. The H atoms again favor fcc hollow sites and level at a height of 1.0 Å above the topmost Rh layer. A fundamental feature of the H-intercalated system is the drastic reduction of the *h*-BN corrugation amplitude by a factor of five from 1.1 Å to 0.2 Å, which supports the picture of H intercalation derived from the experimental results. A gradual growth of the *h*-BN layer height was found for increasing amounts of H atoms, where the mean distance between the *h*-BN layer and Rh increases from about 2.9 Å for the pristine *h*-BN/Rh(111) to about 3.4 Å for *h*-BN/Rh(111) intercalated with 1 ML H atoms. This structural change directly influences the electrostatic potential the corrugation amplitude of which drops from 480 meV to 180 meV at a distance of 3.9 Å above the *h*-BN layer. Thus the strength of the lateral dipole rings in the *h*-BN layer, which are located at the sites of the highest corrugation gradient (rims) and which are the source of the molecular traps of the *h*-BN/Rh(111) nanomesh, is expected to be reduced by about 90 %.[6]

In conclusion, we have shown that exposure of a single layer of hexagonal boron nitride on Rh(111) to atomic hydrogen leads to a change of the surface texture where the corrugation of the sp^2 layer vanishes. This flattening is accompanied by a strong change of the electronic structure of *h*-BN/Rh(111). In the flat state, at least one H atom is captured between four (1×1) *h*-BN/Rh(111) units. Mild annealing results in recovery of the original surface texture of the *h*-BN/Rh(111) nanomesh. Regarding similar sp^2-hybridized template systems such as graphene on Ru(0001), which is the metallic analogue of the nanomesh, it will be interesting to see whether comparable switching behavior occurs.

Experimental Section

STM was performed at $T=350$ K in an Omicron VT-STM where atomic hydrogen was created through dissociation of molecular hydrogen at a hot W filament and dosed on the sample through a nozzle. Photoemission data were recorded in a modified VG ESCALAB 220[16] using monochromatized He I_α radiation with a photon energy of 21.2 eV. In the photoemission experiment, a highly effective doser was used, in which a hot W capillary tube directs a well collimated beam of atomic hydrogen or deuterium on the sample surface.[17] Thermal desorption spectra were recorded with a Prisma QMS 200M2 quadrupole mass spectrometer (Pfeiffer Vacuum) in the channeltron mode. The pumping speed of the TMU 071 P turbomolecular pump (Pfeiffer Vacuum) was 42 L s^{-1} H_2 and 50 L s^{-1} D_2, from which speeds we interpolated 46 L s^{-1} for HD. The *h*-BN/Rh(111) nanomesh was grown following the method described in ref. [4].

Computational methods: The structural and electronic properties of the *h*-BN/Rh(111) were investigated through an atomistic model using DFT. As an initial configuration for the structure optimizations, a four-layer Rh slab with 12×12 replicas of the 2D Rh(111) unit cell using the bulk Rh lattice constant of $a_{Rh}=3.801$ Å plus one layer of hexagonal boron nitride containing 13×13 replicas of the *h*-BN unit cell stretched to match the 12×12 Rh(111) units were used. An effective vacuum region of 25 Å was added to prevent any spurious interaction among periodic images. All the coordinates except the in-plane coordinates of the lowest Rh layer atoms were relaxed. The electronic structure was computed in the framework of the hybrid Gaussian and plane wave scheme (GPW),[18,19] as implemented in the CP2K package[20] using the supercell obtained from the structure optimization. The revised Perdew–Burke–Ernzerhof (revPBE) exchange-correlation functional in the generalized gradient approximation (GGA),[21] adding the dispersion correction arising from Grimme,[22] Molopt local basis sets,[23] and GTH pseudopotentials[24] were used. Visual molecular dynamics (VMD) was used for rendering high resolution representations from the structure optimization results.[25]

Received: February 22, 2010
Published online: July 14, 2010

Keywords: intercalations · isotope effects · monolayers · nanostructures · rhodium

[1] M. S. Dresselhaus, G. Dresselhaus, *Adv. Phys.* **1981**, *30*, 139–326.
[2] T. A. Land, T. Michely, R. J. Behm, J. C. Hemminger, G. Comsa, *Surf. Sci.* **1992**, *264*, 261–270.
[3] C. Oshima, A. Nagashima, *J. Phys. Condens. Matter* **1997**, *9*, 1–20.
[4] M. Corso, W. Auwärter, M. Muntwiler, A. Tamai, T. Greber, J. Osterwalder, *Science* **2004**, *303*, 217–220.
[5] Y. Pan, D.-X. Shi, H.-J. Gao, *Chin. Phys.* **2007**, *16*, 3151–3153.
[6] H. Dil, J. Lobo-Checa, R. Laskowski, P. Blaha, S. Berner, J. Osterwalder, T. Greber, *Science* **2008**, *319*, 1824–1826.
[7] T. Brugger, S. Günther, B. Wang, J. H. Dil, M.-L. Bocquet, J. Osterwalder, J. Wintterlin, T. Greber, *Phys. Rev. B* **2009**, *79*, 045407.
[8] S. Berner, M. Corso, R. Widmer, O. Groening, R. Laskowski, P. Blaha, K. Schwarz, A. Goriachko, H. Over, S. Gsell, M. Schreck, H. Sachdev, T. Greber, J. Osterwalder, *Angew. Chem.* **2007**, *119*, 5207–5211; *Angew. Chem. Int. Ed.* **2007**, *46*, 5115–5119.
[9] J. Zhang, V. Sessi, C. H. Michaelis, I. Brihuega, J. Honolka, K. Kern, R. Skomski, X. Chen, G. Rojas, A. Enders, *Phys. Rev. B* **2008**, *78*, 165430.
[10] A. B. Preobrajenski, A. S. Vinogradov, M. L. Ng, E. Cavar, R. Westerstrom, A. Mikkelsen, E. Lundgren, N. Mårtensson, *Phys. Rev. B* **2007**, *75*, 245412.
[11] A third phase which has been observed in further STM images (not shown) consists of a crumpled *h*-BN layer in which the original nanomesh is still visible at a few places. This phase is the intermediate level where insufficient H intercalation led to a nanomesh corrugation that is not yet fully switched off.
[12] P. Sessi, J. R. Guest, M. Bode, N. P. Guisinger, *Nano Lett.* **2009**, *9*, 4343–4347.
[13] R. Widmer, S. Berner, O. Gröning, T. Brugger, J. Osterwalder, T. Greber, *Electrochem. Commun.* **2007**, *9*, 2484–2488.
[14] R. Laskowski, P. Blaha, T. Gallauner, K. Schwarz, *Phys. Rev. Lett.* **2007**, *98*, 106802.
[15] M. Fukuoka, M. Okada, M. Matsumoto, S. Ogura, K. Fukutani, T. Kasai, *Phys. Rev. B* **2007**, *75*, 235434.

[16] T. Greber, O. Raetzo, T. J. Kreutz, P. Schwaller, W. Deichmann, E. Wetli, J. Osterwalder, *Rev. Sci. Instrum.* **1997**, *68*, 4549 – 4554.
[17] C. Eibl, G. Lackner, A. Winkler, *J. Vac. Sci. Technol. A* **1998**, *16*, 2979 – 2989.
[18] G. Lippert, J. Hutter, M. Parrinello, *Mol. Phys.* **1997**, *92*, 477 – 487.
[19] J. Van de Vondele, M. Krack, F. Mohamed, M. Parrinello, T. Chassaing, J. Hutter, *Comput. Phys. Commun.* **2005**, *167*, 103 – 128.
[20] CP2K, http://cp2k.berlios.de/, **2009**.
[21] Y. Zhang, W. Yang, *Phys. Rev. Lett.* **1998**, *80*, 890 – 890.
[22] S. Grimme, *J. Comput. Chem.* **2004**, *25*, 1463 – 1473.
[23] J. Van de Vondele, J. Hutter, *J. Chem. Phys.* **2007**, *127*, 114105.
[24] S. Goedecker, M. Teter, J. Hutter, *Phys. Rev. B* **1996**, *54*, 1703 – 1710.
[25] W. Humphrey, A. Dalke, K. Schulten, *J. Mol. Graphics* **1996**, *14*, 33 – 38.

